

Zooplankton Distribution and Transport in the California Current off Oregon

The Faculty of Oregon State University has made this article openly available.
Please share how this access benefits you. Your story matters.

Citation	Wu, D, Zhou, M., Pierce, S. D., Barth, J. A., & Cowles, T. (2014). Zooplankton distribution and transport in the California Current off Oregon. Marine Ecology Progress Series. doi:10.3354/meps10835
DOI	10.3354/meps10835
Publisher	Inter-Research
Version	Accepted Manuscript
Terms of Use	http://cdss.library.oregonstate.edu/sa-termsfuse

1
2
3
4
5
6
7
8
9
10
11
12
13
14
15
16
17
18
19
20
21
22
23
24

Zooplankton Distribution and Transport in the California Current off Oregon

Wu D.¹, Zhou M.^{1*}, Pierce S.D.², Barth J.A.², Cowles T.²

¹ University of Massachusetts Boston, 100 Morrissey Blvd, Boston, MA 02125, USA

² Oregon State University, 104 Kerr Administration Building, Corvallis, OR 97331

Key words: Shelf · Coastal retention · Physical-biological coupling · Productivity

* Corresponding author email: meng.zhou@umb.edu

Present address: University of Massachusetts Boston, 100 Morrissey Blvd, Boston, MA
02125, USA

25 **ABSTRACT:** The transport and retention of zooplankton biomass in the shelf and
26 slope regions off Oregon were studied in June 2002. A towed undulating instrument
27 package was used with 2 pairs of Conductivity–Temperature–Depth (CTD) sensors, a
28 fluorometer and an Optical Plankton Counter (OPC) for high resolution
29 measurements of temperature, salinity, depth, fluorescence and zooplankton
30 abundance. The shipboard 153 kHz Acoustic Doppler Current Profiler (ADCP) was
31 used for current measurements in water column. Two different analytical methods
32 for the geostrophic current fields based on ADCP current measurements were
33 employed based on minimizing current divergence. Results revealed high
34 zooplankton biomass values in coastal upwelling areas on the shelf and exchanges
35 between shelf waters with high zooplankton biomass and offshore waters with low
36 zooplankton biomass by crossing-isobath currents. In the shelf area of Heceta Bank
37 off Newport, Oregon shallower than the 153 m isobaths bounded between 41°44'N
38 and 44°37'N, the standing zooplankton biomass was approximately 4×10^4 ton C. The
39 major flux of zooplankton biomass into the area occurred at the northern boundary at
40 a rate of $1 - 2.5 \times 10^3$ ton C d⁻¹ or a specific rate of 0.03–0.06 day⁻¹ based on two
41 different analytical methods; the flux at the southern boundary is one order of
42 magnitude less than that of the northern boundary; and the significant flux out of the
43 area occurred at the 153 m isobath at a rate of $0.8 - 3.7 \times 10^3$ ton C d⁻¹ or a specific rate
44 of 0.02–0.09 day⁻¹. These rates are comparable with the zooplankton growth and
45 mortality rates of approximately 0.1 day⁻¹ reported in literatures within this region.
46 The offshore transport of zooplankton contributes significantly to biomass losses in
47 shelf ecosystems and in turn fuels offshore ecosystems.

48

INTRODUCTION

49 High productivities and their association with mesoscale physical features in the California
50 Current system off the Oregon and California coasts during spring and summer upwelling
51 seasons have led to a number of scientific studies of physical, chemical and biological processes
52 and the sustainability of fisheries associated with human activities. The Coastal Ocean
53 Dynamics Experiment in the early 1980s revealed that the intensive offshore jets associated with
54 cold filaments penetrated more than 100 m deep and transported coastal biota from the shelf to
55 hundreds of kilometers off the shelf (Korso & Huyer 1986). The data from the Ocean Prediction
56 Through Observations, Modeling, and Analysis Experiment in 1982–1986 showed that surface
57 jets and eddies were more energetic in the summer than those in the winter (Rienecker & Mooers
58 1989; Strub et al. 1991). The Coastal Transition Zone Experiment in the late 1980s concluded
59 that the cold filaments were originated from continuous, meandering jets which separated
60 onshelf and offshelf waters (Strub et al. 1991), and deep phytoplankton layers in the offshelf
61 water were originated from the subducted coastal cold water at the transition or converging zone
62 (Brink & Cowles 1991). In the early 1990s, the Northern California Coastal Circulation Study
63 discovered that the velocity variability on time scales from weeks to months was produced by
64 mesoscale eddies impinging off the shelf (Magnell & Winant 1993). The Eastern Boundary
65 Current Project was conducted in the early 1990s, focusing on mesoscale physical and biological
66 fields. Results from this project indicated that maxima of zooplankton abundance and biomass
67 coincided with mesoscale eddies (Huntley et al. 1995). Processes of zooplankton transport and
68 population dynamics associated with these mesoscale eddies were further studied using the size-
69 structured zooplankton model and objective interpolation method (Zhou & Huntley 1997; Zhou
70 2001). These results revealed that generation time scale of mesozooplankton and

71 macrozooplankton varies from 30 to 100 days (Huntley & Lopez 1992). Assuming the current of
72 approximately 10 cm s^{-1} , the advective time scale over a mesoscale or topographic feature of 50–
73 100 km is approximately 6–12 days which is much smaller than the generation time scales
74 (Huntley & Lopez 1992; Zhou 2001). Thus, the effects of advection process on zooplankton
75 distribution and productivity are expected to be on the first order.

76 The California Current is generally southward close and parallel to the coast north of
77 Newport, Oregon (Barth et al. 2000, 2005). It is topographically influenced forming mesoscale
78 eddies or meanders over Heceta Bank entrapping the upwelled cold water near the coast.
79 Frequently mesoscale eddies and filaments spin off from the coast and translate westward. The
80 California Current separates from Cape Blanco and flows southwestward (Kosro et al. 1991;
81 Barth et al. 2000). A subsurface northward undercurrent of 5 cm s^{-1} was observed between 35°N
82 and 50°N along the shelf break in the depth range from 125 and 325 m (Pierce et al. 2000). In
83 the upper 200 m, the vertical integrated volume transports of the southward California Current
84 and the northward undercurrent are approximately 3 and 0.8 Sv, respectively (Barth et al. 2000;
85 Pierce et al. 2000). The dynamics of these mesoscale features are associated with baroclinic
86 instability of the California Current (Pierce et al. 1991), topographic features (Haidvogel et al.
87 1991), and wind stress (McCreary et al. 1991). Biological processes are coupled with mesoscale
88 physical processes in the California Current (Huntley et al. 1995; Zhou & Huntley 1997; Barth et
89 al. 2002). Phytoplankton and zooplankton biomasses enhanced by upwelling in coastal areas
90 will be either transported by the California Current, or retained by eddies and meanders.

91 To understand the fate of zooplankton in eddies and jets requires resolving zooplankton
92 distributions and processes at the scales of eddies and jets. Significant efforts have been made in
93 the last 2 decades using towed optical and acoustic devices to resolve both physical and

94 biological fields at the same location and time. For example, in the California Current system,
95 studies were conducted on correlations between zooplankton maxima, jets and eddies (Huntley et
96 al. 1995; Zhou 2001; Barth et al. 2002); in the Georges Bank region, studies focused on the
97 zooplankton recruitment and their cross-front transport mechanisms (Wiebe et al. 2001; Benfield
98 et al. 2003; Ullman et al. 2003); and in northern Norwegian shelf areas, studies centered on
99 onshore intrusions of zooplankton and their impacts on local productivity (Fossheim et al. 2005;
100 Zhou et al. 2009; Zhu et al. 2009). Though results from these early studies elucidated qualitative
101 relationships between physical and biological fields, quantitative estimates of transport and
102 retention of zooplankton biomass and zooplankton process rates were rarely found. Without
103 resolving the physical processes of advection and retention, population dynamic processes of
104 zooplankton will not be resolved.

105 A cruise was conducted between June 1 and 17 2002, as a part of the United States (US)
106 Global Ocean Ecosystems Dynamics Program (GLOBEC) Northeast Pacific Study (NEP) for
107 surveying physical and biological fields using towed and shipboard physical–biological sensors
108 (Barth et al. 2005). These integrated physical and biological data allowed us to make
109 quantitative estimates of transport, retention and process rates, potential errors based on different
110 analytical methods, and limits of survey and analytical methods. These results then allow us to
111 access local food web dynamics.

112 **DATA AND METHODS**

113 **Data**

114 The study area was designed from 44°37'N off Newport, Oregon to 41°44'N off Crescent
115 City, California and from the coast to approximately 100 km offshore (Fig. 1). The mesoscale
116 survey was conducted in a period of 5 days with 12 cross–shelf transects approximately

117 0.25° apart in the latitude. Two fine-scale surveys were then conducted in the Heceta Bank and
118 Cape Blanco regions with a latitudinal interval of approximately 0.05–0.15°. A towed SeaSoar
119 instrument package was employed during the survey including 2 pairs of SBE 911 plus
120 conductivity, temperature and depth sensors (CTD; Sea-Bird Electronics, Inc.) for the
121 hydrographic data, a fluorometer (Wet Lab) for relative fluorescence and an Optical Plankton
122 Counter (OPC; Focal Technologies) for zooplankton between 0.25 and 2.4 cm in Equivalent
123 Spherical Diameter (ESD). The SeaSoar undulated from the surface to approximately 10 m
124 above the bottom in coastal areas, or a maximum depth of approximately 200 m in offshore areas
125 at a ship speed of 7–8 knots. The SeaSoar undulating cycle varied from 1.5 min on the shelf to
126 16 min off the shelf which led to horizontal resolutions of 350 m and 4 km on and off the shelf,
127 respectively. The highest vertical resolutions of physical and biological data were determined by
128 the SeaSoar undulation speed and sampling rates of CTD at 24 Hz, and both Fluorometer and
129 OPC at 2 Hz. Due to the OPC failure, there were no OPC data collected on transects 8–12 of the
130 mesoscale survey.

131 A vessel mounted 153 kHz Narrow Band (NB) Acoustic Doppler Current Profiler (ADCP;
132 RD Instruments) was used for current measurements with the bin length of 8 m and ensemble
133 average of 5 min. The error in 5-minute averaged velocities was 0.04 m s^{-1} and 0.02 m s^{-1} using
134 navigation and bottom track, respectively (Barth et al. 2005). Wind measurements were obtained
135 from NOAA National Data Center buoy 46050 located at $44^{\circ}37' \text{N}$, $124^{\circ}30' \text{W}$, approximately 37
136 km offshore of Newport, Oregon (www.ndbc.noaa.gov). For zooplankton taxonomic
137 information, live samples were collected on May 31 2002 over Heceta Bank (Fig. 1) by using a
138 0.5 m^2 ring net with $202 \mu\text{m}$ mesh towed in the upper 100 m at 1 knot (Courtesy of W. Peterson,
139 NOAA NW Fisheries Science Center).

140

Data processing

141 The OPC provides plankton counts in 3494 digital sizes corresponding to a size range
142 between 0.25 and 24 μm in ESD (Herman 1992). For using the carbon unit, the ESD of a
143 zooplankton was converted to its body carbon based on the equation of Rodriguez and Mullin
144 (1986) developed specially for California Current system by assuming the length to width aspect
145 ratio of 1.61 for copepods (Huntley et al. 2002), i.e.,

$$146 \quad \log_{10}(\mu\text{gC}) = 2.23\log_{10}(\text{ESD in } \mu\text{m}) - 5.58. \quad (1)$$

147 To increase the statistics of measurements in a given size interval, 3494 body carbon sizes were
148 integrated into 50 body carbon size intervals on an equal \log_{10} basis. Within each size interval,
149 accumulative biomass ($\mu\text{g C}$) of zooplankton was computed for every 0.5 s, and then normalized
150 by the water volume filtered (m^3) and size interval (μgC) that leads to a normalized biomass
151 spectrum in the unit of m^{-3} following Platt and Denman (1978) and Zhou and Huntley (1997)
152 (referred to hereafter as biomass spectrum). All OPC data were processed along the undulating
153 paths for the mesoscale and fine-scale surveys. It should be kept in mind that the uncertainty of
154 OPC in estimating zooplankton biomass due to different optical properties of zooplankton
155 species and spatial variation of taxonomic compositions may significantly affect zooplankton
156 biomass estimates though this manuscript focuses on effects of physical processes on process
157 rate estimates (Herman 1992; Huntley et al. 1995).

158 To compute coupled physical and biological data and variables, all CTD, fluorometer and
159 OPC data were further processed into 8 m vertical bins to match the ADCP data. Because the
160 first depth bin of ADCP measurements started from 25 m, all CTD, fluorometer and OPC data in
161 the upper 25 m were averaged. Then at each depth bin, all data were interpolated into 50×50
162 horizontal grids by using the Objective Interpolation method within the survey area bounded by

163 41°54'N–44°40'N and 124°08'W–125°46'W (Fig. 1) (Bretherton et al. 1976; Zhou 1998; Barth
164 et al. 2000).

165 The spatial decorrelation scales and covariance functions were determined from the
166 autocorrelations of temperature data from CTD in the zonal and meridional directions based on
167 Legendre (1983). The zonal correlations were computed at individual longitudinal transects, and
168 then the mean zonal correlation was obtained by taking a latitudinal average. For the mean
169 meridional correlation, we first binned the data into 0.15° longitudinal bins along each transect,
170 computed the meridional correlation at a given longitude, and then averaged meridional
171 correlations longitudinally. The minimum scale of physical and biological features in the
172 latitude was determined by the distance between two transects approximately 0.25°. The results
173 indicated an anisotropic field with the decorrelation scales of 33 km and 88 km in the zonal and
174 meridional directions, respectively (Fig. 2), both of which are much larger than the spatial
175 resolutions in the datasets. The decorrelation scales were consistent with that estimated from the
176 time series of current data off Oregon (Kundu & Allen 1976). An appropriate covariance
177 function $(1-r)e^{-r}$ was selected to fit autocorrelation data where r is equal to $\sqrt{(\Delta x/l_x)^2 + (\Delta y/l_y)^2}$,
178 and l_x and l_y are the decorrelation scales in the zonal and meridional directions, and Δx and
179 Δy are the distances between two locations in the longitude and latitude.

180 To remove barotropic tidal current components from ADCP current measurements is
181 challenging because errors can be introduced by measurements, predicted tidal currents from a
182 tidal model and interpolation method used for gridding. The predicted tidal currents from a tidal
183 model were extracted based on the location and time along the ship track (Erofeeva et al. 2003),
184 and the detided currents were obtained by subtracting the predicted tidal currents from the ADCP
185 current measurements. Because there is no streamfunction for tidal currents, fitting a

186 streamfunction to detided currents during interpolation will further remove tidal and
187 ageostrophic components. We used two objective interpolation methods developed by Barnes
188 (1964) and Bretherton et al. (1976) (Referred to hereafter as Barnes and BDF interpolations,
189 respectively). Barnes interpolation is a successive correction method by minimizing differences
190 between passes under defined decorrelation scales. The streamfunction was then calculated
191 based on Hawkins and Rosenthal (1965). BDF interpolation is based on statistics and defined
192 decorrelation scales, and the streamfunction is obtained by minimizing divergences (Bretherton
193 et al. 1976; Dorland & Zhou 2007). Although these two mathematical interpolations are all valid
194 and well tested, the differences in results between these two different methods will bring insight
195 into the sensitivities and uncertainties for interpreting population dynamic processes.

196 We tested two spatial covariance functions for Barnes interpolation of which one is an
197 isotropic covariance function with decorrelation scales of 50 km in both zonal and meridional
198 directions to match previous studies (Huntley et al. 1995), and another is anisotropic covariance
199 function with decorrelation scales of 33 km in the zonal direction and 88 km in the meridional
200 direction which match the decorrelation scales computed from our data. Two passes were
201 applied for both covariance functions and the velocity differences between two passes are less
202 than 1 cm s^{-1} . We found no significant differences in results between these two different
203 covariance functions. For the consistency with previous studies the results from the isotropic 50
204 km Barnes interpolation are presented in this paper. Because BDF interpolation turns to
205 maximize mesoscale features at the defined spatial scales, we used the anisotropic covariance
206 function with scales of 33 km in the zonal direction and 88 km in the meridional direction. The
207 numerical divergences of interpolated current fields are in the order of 10^{-7} s^{-1} and 10^{-18} s^{-1} for
208 Barnes and BDF interpolations, respectively.

209

Transport theories

210 For zooplankton biomass (b), the local change is primarily determined by the convergence
211 of biomass transport, and the bio–reaction related to the population dynamics processes, i.e.,

$$212 \quad \frac{\partial b}{\partial t} = R(b, t) - \left(\frac{\partial ub}{\partial x} + \frac{\partial vb}{\partial y} + \frac{\partial wb}{\partial z} \right), \quad (2)$$

213 where t is the time, and u , v , and w are the zonal (x), meridional (y) and vertical (z) velocity
214 components, respectively. On the right side of Eq. (2), $R(b, t)$ represents the bio–reaction, a net
215 production, and the second term presents the advection or convergence of zooplankton
216 transports. In order to examine the total biomass variation, we integrate Eq. (2) over the water
217 column (H) assuming there is no flux crossing the surface and bottom, we will have

$$218 \quad \frac{\partial}{\partial t} \int_H^0 b dz = \int_H^0 R(b, t) dz - \left(\frac{\partial}{\partial x} \int_H^0 u b dz + \frac{\partial}{\partial y} \int_H^0 v b dz \right). \quad (3)$$

219 In Eq. (3), on the left side the term is the local change rate of vertically–integrated biomass in the
220 water column, and on the right side the first and second terms are the bio–reaction and
221 convergence of horizontal transport, respectively. The horizontal transport can be calculated
222 directly from binned current and OPC data. The horizontal convergence of biomass can be
223 further separated into two terms as,

$$224 \quad - \left(\frac{\partial}{\partial x} \int_H^0 u b dz + \frac{\partial}{\partial y} \int_H^0 v b dz \right) = - \int_H^0 \left(u \frac{\partial b}{\partial x} + v \frac{\partial b}{\partial y} \right) dz - \int_H^0 b \left(\frac{\partial u}{\partial x} + \frac{\partial v}{\partial y} \right) dz. \quad (4)$$

225 On the right side, the first term is the biomass convergence contributed by gradient advection,
226 and the second term is the retention of b determined by current convergence. This current
227 convergence term should be small because the flow field at the spatial scale of our interests is

228 nearly geostrophically balanced (Kosro & Huyer 1986; Pickett et al. 2003; Shearman et al.
 229 2000). The current convergence estimates resulted from the Ekman pumping driven by wind
 230 stress curl and from the secondary circulation determined by the quasi-geostrophic dynamics are
 231 on the second order. Thus, in a heterogenic zooplankton field, the advection of zooplankton
 232 gradients should play the dominant role in concentrating or dissipating zooplankton.

233 The sign of the biomass gradient advection implies a high biomass or a low biomass center
 234 moving into an area. When a positive (negative) current advects a negative (positive) gradient,
 235 the higher biomass is moving in which we refer as a positive gradient advection. When a
 236 positive (negative) current advects a positive (negative) gradient, the lower biomass is moving in
 237 which we refer as a negative gradient advection.

238 To examine the productivity of a given region, a Eulerian control water volume (V) can be
 239 selected. For example, a control water volume of Oregon coastal region can be bounded by
 240 Transects 1 and 12 in the latitude, the coast and 153 m isobath in the longitude, and the surface
 241 and bottom in the vertical. Integrating Eq. (3) over an area (S) bounded by the boundary (δS)
 242 and water depth (H), and applying Stokes' theory (Beyer 1987), we have

$$243 \quad \frac{\partial}{\partial t} \int_S \int_H (bdz) dS = \int_S \int_H [R(b,t) dz] dS - \oint_{\delta S} \left[\left(\int_H^0 ubdz \right) dy + \left(\int_H^0 vbdz \right) dx \right]. \quad (5)$$

244 Eq. (5) again represents the balance between biomass change in a control region, local net
 245 production and transport fluxes.

246 The errors during estimating biomass transports are contributed from errors in both currents
 247 and zooplankton biomass estimates. Theoretically, the errors of those estimated streamfunctions
 248 and zooplankton distributions should be known because those interpolations are based on

249 statistics and given covariance functions (Bretherton et al. 1976; Barth et al. 2000). However,
250 the detided ADCP current measurements include unknown errors in ship movements, modeled
251 tidal currents and ageostrophic currents. Zooplankton measurements include unknown errors
252 due to zooplankton patchiness, migration behavior and avoidance. Though these errors could be
253 small as indicated, we do not know them quantitatively and their statistical characteristics, and
254 cannot resolve these errors in our datasets and progresses of these errors in Eq. (5).

255 **RESULTS**

256 **Wind condition**

257 The wind during the survey period (June 2–15 2002) was predominately southward,
258 upwelling–favorable with a maximum wind speed of approximately 10 m s^{-1} (Fig. 3). There
259 were two northward wind events on June 4 and 13 2002. The first event approximately 2 days
260 occurred in the second half of the mesoscale survey, and the second event less than 2 days
261 occurred in the southern fine–scale survey. The predominated upwelling favorable wind, short–
262 term relaxation and downwelling favorable wind led upwelling and downwelling.

263 **Horizontal distributions of temperature, currents, chlorophyll, and zooplankton**

264 The results from the autocorrelation analysis of CTD data indicate an anisotropic field
265 (Fig. 2). In the zonal direction, the autocorrelation decreases quickly within 18 km, becomes flat
266 between 18 and 27 km, and has the first zero–crossing at 33 km, which implies there were
267 multiple scales. In the meridional direction, the autocorrelation decreases monotonically
268 crossing the zero at 88 km. The fits using different theoretical functions were tested. The
269 covariance function of $(1-r)e^{-r}$ was the best–fit and chosen for the interpolations of temperature,
270 chlorophyll, zooplankton abundance and biomass, and currents (Figs. 4–9).

271 The coastal upwelling area can be identified from the colder water at the surface along the
272 Oregon and northern California coasts compared to the warmer water in the offshore areas (Fig.
273 4). Between Newport and Cape Blanco, Oregon, the upwelling area was parallel to the coast
274 within a narrow 10–20 km band while south of Cape Blanco, the upwelling area extended
275 offshore–ward approximately 100 km. Associated with these upwelling fronts, the currents from
276 streamfunctions best–fitted with the detided currents from the mesoscale survey have revealed
277 jets and eddies (Fig. 5). On Heceta Bank, the cold water of 10°C started inshore and spread over
278 the bank area. South of Cape Blanco, associate with the broad upwelling area, the California
279 Current departed from the coast to the southwestward. From Barnes interpolation, the California
280 Current was steered offshore at Heceta Bank and Cape Blanco forming meanders (Fig. 5b) while
281 from BDF interpolation, eddies were clearly formed over Heceta Bank and off Cape Blanco (Fig.
282 5c). The results from these two interpolations are significantly different due to different inherent
283 assumptions in methods. Though both results are valid because both interpolation methods are
284 well developed and tested, the significant differences in results have demonstrated the challenges
285 in resolving physical processes and transport–retention of zooplankton populations.

286 Because the OPC was failed in the second half mesoscale survey, we used the CTD,
287 fluorometer and OPC data from the mesoscale survey transects 1–7 and the southern fine–scale
288 survey transects (Fig. 1). The chlorophyll distribution at 5 m was highly correlated with the
289 upwelled cold water while the zooplankton biomass distribution at 5 m was not correlated with
290 the upwelled cold water (Fig. 4). Elevated chlorophyll and zooplankton concentrations were
291 found in the mesoscale eddy and the offshore transported cold water near Heceta Bank, and in
292 the broad upwelling area south of Cape Blanco. The offshore transports of phytoplankton and
293 zooplankton by the California Current were found west of Heceta Bank while the offshore water

294 with low chlorophyll and zooplankton concentrations intruded into the coastal area between
295 Heceta Bank and Cape Blanco.

296 The spatial patterns in the mean zooplankton abundance and biomass distributions
297 between the surface and 153 m can visually be linked to the temperature patterns and mesoscale
298 features of jets and eddies (Fig. 6). High zooplankton abundances and biomass were found along
299 all coastal upwelling areas implying the effects of upwelling on primary and secondary
300 productions. Zooplankton abundance maxima were found in most coastal areas while
301 zooplankton biomass maxima were found only over Heceta Bank and Coos Bay areas.

302 **Vertical distributions of temperature, currents, chlorophyll and zooplankton**

303 The coastal upwelling and offshore stratification can be seen from the outcropped
304 thermocline along mesoscale Transect 5 (Fig. 7). The upwelling area was limited near the coast
305 with the temperature as low as 7–8°C. Crossing the upwelling front, the water was stratified
306 with the surface temperature of 12–14°C and the thermocline depth of 20–30 m. The ADCP
307 current measurements are superimposed on the temperature transect indicating the jets and
308 eddies associated with slopes of thermocline.

309 Between 125° 00'W and 125° 15'W on this transect, a jet was found southwestward at
310 approximately 30 cm s⁻¹ consistent with the offshore-ward California Current steered by Heceta
311 Bank (Fig. 5) (Barth et al., 2005). The along transect current component shows a convergent
312 pattern in the depth range over 180 m occurring within this jet. This zonal convergence may lead
313 to the deep penetration of phytoplankton and zooplankton biomasses (Fig. 7).

314 The surface chlorophyll maximum was found in the nearshore upwelling area (Fig. 7), and
315 the subsurface maxima were found near thermocline areas in the offshore stratified water column.

316 Corresponding to such phytoplankton distributions, zooplankton were distributed over the entire
317 water column with surface enhancements in the nearshore area, and strongly correlated with
318 phytoplankton maxima in offshore areas.

319 **Zooplankton biomass transport**

320 The horizontal transport vectors of zooplankton biomass within the upper 153 m are
321 calculated based on OPC biomass measurements and 2 current fields from Barnes and BDF
322 interpolations (Fig. 8). All of them show similar large-scale patterns, for example, the dominant
323 offshore and southward transports of zooplankton. The onshore and northward transports of
324 zooplankton were revealed only at the mesoscale.

325 The depth integrated zooplankton biomass gradient advection is calculated based on Eq. (4)
326 using the OPC biomass measurements and the mesoscale current field based on BDF
327 interpolation (Fig. 9a). Positive advection implies that higher biomass water mass is displacing
328 the lower biomass water mass, and vice versa. Negative advection was found in the onshore
329 current south of Heceta Bank where the shoreward current transported low biomass water
330 northeastward. Positive values were found in coastal regions where the currents had transported
331 higher zooplankton biomass into the area. Within the advection terms as expressed in Eq. (4),
332 the advection of biomass gradients dominated the processes, especially in the areas of offshore
333 transport. To compare the biomass advection with zooplankton growth rates, the specific
334 convergence rate of biomass advection is computed by the ratio of depth integrated biomass
335 gradient advection to depth integrated zooplankton biomass in the survey area (Fig. 9b). The
336 convergence rate varies between -0.5 and 0.5 day^{-1} in June, the early summer season, indicating
337 the importance of physical advective processes on zooplankton distributions.

338 To estimate the magnitude of zooplankton biomass offshore transport and coastal retention,
339 we define a coastal area by the 153 m isobath and survey Transects 1 and 12 (Fig. 1). Assuming
340 there was no flux crossing the coast, the transport fluxes crossing northern, western and southern
341 boundaries in Eq. (5) were estimated based on the current fields from both Barnes and BDF
342 interpolations (Table 1). The results show the flux estimates are extremely sensitive to the
343 current fields, especially the estimates at 153 m isobath.

344 **Zooplankton size structure**

345 To investigate zooplankton size structures and species, 6 representative areas are selected in
346 the survey area (Fig. 6a): Area 1 represents the offshelf low biomass area west of Heceta Bank,
347 Area 2 is the high productive Heceta Bank region, Area 3 is in the offshore-ward jet off Heceta
348 Bank with both chlorophyll and zooplankton maxima, Area 4 is in the offshelf water with both
349 low chlorophyll and zooplankton, Area 5 represents the nearshore chlorophyll and zooplankton
350 biomass maxima off Cape Blanco, and Area 6 is within the offshore jet with both chlorophyll and
351 zooplankton maxima southwest of Cape Blanco. The biomass spectra in Fig. 10a–c are paired
352 between offshelf Areas 1 and 4, between nearshore Areas 2 and 5, and offshore jet Areas 3 and 6.

353 To evaluate the effects of zooplankton vertical migration on zooplankton distributions, the
354 OPC data were separated into day and night time based on PAR (photosynthetically available
355 radiation) which was predicted as a function of latitude and Julian day. The night period was
356 defined as PAR equal to zero corresponding to the local time approximately between 19:00 and
357 05:00 h during the survey period. Daytime and nighttime biomass spectra were constructed
358 between the surface and the maximum depth the SeaSoar reached (Fig. 10d). We exclude the
359 coastal area shallower than 153 m isobath for this study because high biomass measurements in
360 shallow coastal regions could lead to high biomass estimates in upper water columns and bias the

361 estimates. The regression relationship between daytime and nighttime biomass spectra indicates
362 the significant similarity ($y = 1.06x - 0.29$, $r^2 = 0.99$).

363 **DISCUSSIONS**

364 **Mesoscale current fields from two interpolation methods**

365 Both Barnes and BDF interpolation methods and stream functions have revealed coastal
366 jets, meanders and eddies (Figs. 5b and 5c). The coastal jets and eddies are significantly steered
367 by shallow banks and capes in the Oregon and northern California section (Brink & Cowles 1991;
368 Barth et al., 2000; Barth et al., 2002). Though both interpolations have provided large scale
369 currents, meanders and eddies, significant differences exist. For example, the California Current
370 was turned to the offshore direction forming large crossing–isobath currents and a meander over
371 Heceta Bank from Barnes interpolation and forming small crossing–isobath currents and an eddy
372 over Heceta Bank from BDF interpolation. Comparing both to the original detided ADCP
373 currents, Barnes interpolation provides a smoother large scale circulation pattern with less
374 mesoscale features while BDF interpolation remains more detailed mesoscale features under the
375 nondivergent condition. The differences in the circulation patterns between different
376 interpolation methods are resulted from the inherent assumptions within the methods.

377 The differences between current fields are critically important in understanding transport
378 and retention mechanisms of biota in coastal areas, for example Heceta Bank. Barnes
379 interpolation has shown a crossing–isobath offshelf transport in the southwestern part of the bank,
380 while BDF interpolation has shown a much reduced crossing–isobath current controlled by
381 isobaths. The magnitude of crossing–isobath currents obviously plays an important role for the
382 population dynamics of zooplankton on Heceta Bank. It is feasible to adjust parameters and
383 methods to converge results from these two different interpolation methods though any

384 subjective adjustment will not make any new understanding. Though both these current fields
385 are valid but focus on different features of the current fields, how can we choose interpolation
386 methods and current fields for computing transport and retention of biological fields? The
387 ultimate test has to compare to observations of both physical and biological fields. These
388 methods are originally developed for analyzing and filtering imperfect field data. New
389 progresses in both observations and analytical methods need to be made for better physical and
390 biological fields.

391 **Zooplankton maxima vs. mesoscale current fields**

392 The meander or eddy over Heceta Bank can remain for several weeks according to
393 Lagrangian drifter studies (Barth et al. 2000; Geen et al. 2000). At Cape Blanco, the California
394 Current separates from the coast, and typically forms jets and eddies (Barth et al., 2000, 2005).
395 These eddies and meanders increase the residence time and in turn can potentially affect
396 phytoplankton and zooplankton productivities. The strong correlations between coastal
397 upwelling, eddies, chlorophyll concentrations and zooplankton biomass are clearly shown in Figs.
398 4, 5 and 6, suggesting that upwelling drives the productive coastal ecosystem off Oregon and
399 northern California. Downwelling wind events did occur during the survey (Fig. 2). Would a
400 downwelling event erases chlorophyll and zooplankton maxima in nearshore areas? In a short
401 downwelling wind event, the downwelling wind could prevent biota from offshore transport and
402 retain biomass along coastal regions by its onshore Ekman transport. Though currents varied
403 between upwelling and downwelling favorable winds, the effect of enhanced productivity in
404 coastal areas was persistent.

405 In offshore areas, the zooplankton biomass maxima were found associated with offshore–
406 ward jets and meanders (Figs. 5 and 6). Some of these maxima could be related to the offshore

407 transport by jets. For example, the deep zooplankton maximum between 125°15'W and
408 124°55'W along Transect 5 (43°45'N) was associated with an offshore-ward jet off Heceta Bank.
409 Offshore transports of phytoplankton and zooplankton biomasses have been observed (Washburn
410 et al. 1991; Huntley et al. 1995, 2000; Barth et al. 2002). Our study further shows the
411 relationship between coastal productive areas and offshore zooplankton maxima associated with
412 offshore-ward jets.

413 **Zooplankton deep maximum**

414 A zooplankton deep maximum was found along Transect 5 (43°45'N) between 125°15'W
415 and 125°50'W in the offshore jet region (Fig. 7). Similar chlorophyll and zooplankton deep
416 maxima were also found in other studies within the California Current system (Huntley et al.
417 2000; Barth et al. 2002). The primary cause of deep biomass maxima has been interpreted as the
418 subduction of coastal biota with subducting waters during offshore transport. In these deep
419 maxima, both coastal and offshore zooplankton species can be found representing the transport
420 and mixing of coastal and offshore waters.

421 The zooplankton deep maximum had a zonal scale of 40 km which is equivalent to the
422 internal Rossby Radius in this area (Chereskin et al. 1994). No zooplankton deep maximum was
423 found in either survey Transect 4 or 6, implying that the meridional scale of this deep maximum
424 is less than 40 km. We can speculate that when jets and eddies are formed at the scale similar to
425 the internal Rossby Radius, their advection of zooplankton gradients can lead to the increase in
426 zooplankton patchiness at the similar scales.

427 The high zooplankton biomass in deep waters should be associated with subduction of
428 surface waters (Barth et al. 2002). Studies of quasigeostrophic dynamics of jets and fronts

429 indicate that denser water tends to slide underneath less dense water (Rudnick 1996; Shearman et
430 al. 2000; Barth et al. 2002). In the offshore-ward currents off Heceta Bank and Cape Blanco, the
431 upwelled deep water near coasts could subduct near upwelling fronts with coastal biota and then
432 be transported offshore with the currents that led to a convergent zone or subduction zone of
433 zooplankton around the currents.

434 There is no significant difference between daytime and nighttime biomass spectra from this
435 study (Fig. 10d). In studies of zooplankton vertical diel migration processes, it was found that
436 krill migrated to the surface layer at the beginning of sunset, and then they spread into a broad
437 water column depending on prey fields (Zhou et al. 2005). It is also found that the migration
438 patterns of mesopelagic boundary communities could be complicated by different migration
439 speeds of different species (Benoit-Bird & Aub 2003). To examine detailed diel migration
440 pattern, the depth center of biomass distribution in the water column was calculated as a function
441 of time. The zooplankton biomass data were binned into 8 m depth bins from the surface to 153
442 m, and then averaged along the ship track within a longitudinal interval of 0.05°. The depth
443 center (Z) of biomass distribution was determined by

$$444 \quad Z = \frac{\sum_i B_i \cdot z_i}{\sum_i B_i}, \quad (7)$$

445 where B_i is the biomass at the depth of z_i . In order to avoid the shallow bottom which could bias
446 the estimates of biomass depth centers, the calculations were also made from individual OPC
447 profiles deeper than 153 m west of 124°48'N (Fig. 12). Taking the hourly averaging, the biomass
448 depth centers varied in the ranges of 54±21 m and 60±21 m during the daytime and nighttime
449 periods, respectively. The two sample t -test ($df = 174$) led to the p -value less than 0.29. Though
450 there is a difference in the depth centers between daytime and nighttime, it is clear that

451 zooplankton did not aggregate in the upper water column more during the night than they did
452 during the day. Previous studies also found that total copepod biomass and individual species
453 showed no day–night difference in both net and OPC samples among the California Current
454 region (Mackas et al. 1991; Huntley et al. 1995; Peterson et al. 2002).

455 **Effects of advection on zooplankton community structure**

456 The biomass spectra from 6 selected areas had the similar feature that is high abundances at
457 small size classes and low abundances at large size classes (Fig. 10). Such a feature has been
458 observed in most of ocean and freshwater environments (Sheldon et al. 1967, 1972; Rodríguez &
459 Mullin 1986; Sprules & Manuwar 1986). Results from net samples collected in the same survey
460 period over Heceta Bank indicate the zooplankton assemblage in the body size range between
461 10^0 and 10^3 μgC in the California Current is dominated by a small number of species similar to
462 previous findings (Huntley et al. 2000). Body sizes between 0.5 and 1100 μgC contained early
463 to adult stages of copepod species, *Pseudocalanus spp.*, *Acartia spp.*, *Centropages spp.*, *Calanus*
464 *marshallae* and *Calanus pacificus*, and early stages of *Euphausia pacifica* and *Sergestes similis*.
465 Body sizes larger than 1100 μgC were dominated by middle to adult stages of *Euphausia*
466 *pacifica*, *Sergestes similes* and *Thysanoessa spinifera* (Mackas et al., 1991; Huntley et al., 2000;
467 Peterson et al., 2002).

468 Among the biomass spectra, the values in the size range between 16 and 250 $\mu\text{g C}$ (1.2–2.4
469 in the \log_{10} scale) over Heceta Bank (Area 2) were higher than those of other areas (Fig. 10).
470 Within this size range, the net tow samples in the same area (124.51°W, 44.25°N) and at the
471 same time indicate a biomass composition of 35% by *Pseudocalanus spp.* and 33% by *Calanus*
472 *mashallae* which are two of the most common copepod species in Oregon upwelling areas (Fig.
473 11) (in courtesy of W. Peterson). Such elevated biomass spectra from the linear relationship have

474 also been found in other coastal regions during spring such as the Norwegian shelf where the
475 elevated biomass spectra were contributed by *Calanus finmarchicus* CV and adults and
476 euphausiid larvae (Zhou 2009).

477 Two types of biomass spectra were observed during the survey: the linear spectra found in
478 the offshore area (Area 1) and along the onshore intruding current (Area 4); and the nonlinear
479 spectra found in coastal upwelling areas (Area 2) and the offshore jets (Area 3). Because the
480 offshore and onshore–ward jets carried the biota from their origins, the spectrum of zooplankton
481 in an offshore jet inherited the dome–shaped biomass spectrum of a coastal cohort and the
482 spectrum in an onshore jet inherited the linear spectrum of an offshore cohort. Thus, the dome–
483 shape of the biomass spectra in the offshore eddies marked by Areas 2 and 3 were contributed by
484 *Pseudocalanus spp.* and *C. mashallae* from coastal upwelling zones. These coastal zooplankton
485 communities can be entrapped in eddies and advected further into offshore region on an order of
486 100 days. The coastal zooplankton communities entrapped in a mesoscale eddy and advected
487 100 km off the shelf were also found (Huntley et al. 1995, 2000).

488 The offshore transport of coastal communities can be seen from the association between
489 extending tongues of high zooplankton biomass from Heceta Bank and Cape Blanco, and the
490 offshore currents (Figs. 5 and 6). In contrast, the onshore currents transported low zooplankton
491 biomass waters to nearshore regions with zooplankton minima, such as the low zooplankton
492 biomass band south of Heceta Bank extending from the offshore region to the coast region
493 corresponding to a negative gradient advection (Fig. 9). In the Heceta Bank region, these
494 onshore and offshore transports led to a biomass convergence.

495

496

Coastal convergence and offshore export of zooplankton biomass

497

498

499

500

501

502

503

504

505

506

507

508

509

510

511

512

513

514

515

516

517

518

The transport flux estimates crossing the boundaries surrounding the coastal region are extremely sensitive to the current fields, especially the estimates at 153 m isobath (Table 1). The current field from Barnes interpolation leads to significant crossing–isobath transport while the current field from BDF interpolation is mostly in parallel to 153 m isobath minimizing the crossing–isobath transport. Based on these estimates, the major transport flux into the Oregon coastal region occurred in the northern boundary (Transect 1) where the California Current transports zooplankton biomass southward approximately 2.5×10^3 and 1.0×10^3 ton C d^{-1} based on Barnes and BDF interpolations, respectively. Across the southern boundary (Transect 12), the transport flux was relatively small and negligible comparing to the northern boundary. The offshore transport across the 153 m isobath was on the same order of magnitude as that across the northern boundary. The offshelf transport across the 153 m isobath computed from the currents based on Barnes interpolation is approximately 3.7×10^3 ton C d^{-1} 4–5 times higher than that of BDF interpolation approximately 0.8×10^3 ton C d^{-1} . The difference in transport estimates primarily occurred at the shelf break south of Heceta Bank. The smaller crossing–isobaths transport from the current field based on BDF interpolation was caused by both the mesoscale currents being more in parallel to the 153 m isobath and the mesoscale returning currents associated with offshore jets. The crossing–isobath transport of biota due to crossing–isobath currents from Barnes interpolation occurs south of Heceta Bank and Cape Blanco.

The total zooplankton biomass integrated within the coastal area shallower than 153 m isobath is approximately 4×10^4 ton C. The net transport crossing the boundaries of this coastal area was -1.4×10^3 and 0.3×10^3 ton C d^{-1} using the current fields derived from Barnes and BDF interpolations leading to the biomass accumulation at the rates of -0.04 and $0.01 d^{-1}$, respectively.

519 The differences between transport fluxes estimated using different interpolation methods do not
520 imply any unreliability of these mathematical methods. The differences indicate the differences
521 between these methods in dealing with uncertainties from field data. Thus to verify results from
522 mathematical methods in field observations is challenging but necessary for us to study coupled
523 physical and biological processes.

524 The growth rate of zooplankton is approximately 0.1 d^{-1} in 8°C water within upwelling
525 areas using a general formula (Huntley & Lopez 1992; Hirst & Bunker 2003; Bi et al. 2010;
526 Zhou et al. 2010), or 0.08 d^{-1} for overall copepod species from a time series in upwelling waters
527 off Newport, Oregon (Gómez-Gutiérrez and Peterson 1999). The local specific convergence
528 rates of biomass advection were between -0.5 and 0.5 day^{-1} which were significantly higher than
529 local zooplankton growth rates (Fig. 9b). The dominance of physical advective processes in
530 zooplankton biomass variations elucidates the difficulty in studying *in-situ* zooplankton
531 population dynamics processes which requires following a specific zooplankton cohort. Though
532 the local convergence rate is dominant 5 times higher than the local growth rate, the area mean of
533 convergence rates becomes less while integrating the convergence rate over a larger region. The
534 accumulation rates due to the convergence of biomass gradient advection in the entire coastal
535 area shallower than 153 m isobaths off Oregon are approximately -0.04 and 0.01 d^{-1} based on 2
536 different interpolations, respectively. These accumulation rates are approximately one order of
537 magnitude smaller than the growth rate, indicating the high zooplankton production in the
538 Oregon coastal region was enhanced by the local primary production.

539 The local convergence of zooplankton transport is dominated by advection of
540 zooplankton gradients because the convergence of currents is secondary. In the survey area, the
541 advection of zooplankton biomass gradients shows alternating negative and positive patches

542 associated with currents and biomass gradients (Fig. 9). The signs simply indicate the advection
543 of a high biomass center or a low biomass center into a local area. In the offshore-ward jets, the
544 positive sign indicates an offshore transport of nearshore-produced zooplankton biota while in
545 an onshore current the negative sign indicates an intrusion of offshore low zooplankton water.
546 Thus, the mosaic of zooplankton gradient advection in Fig. 9 also represents the horizontal
547 exchange-mixing processes of zooplankton nearshore and offshore biota due to advective
548 transports. These results, especially the different estimates using Barnes and BDF interpolations,
549 elucidate the nonlinearity of zooplankton gradient advection processes, and potential biases by
550 linear averaging removing mesoscale features. Can we improve measurements of currents and
551 biomass so that estimates of advection and population process rates can be improved? What a
552 research vessel can do is limited by its cruise speed and limited sensors can be deployed at the
553 same time. The recent development of autonomous underwater vehicles and miniaturized optical
554 and acoustic sensors may provide the mean to resolve higher spatial and temporal resolution
555 physical and biological fields, and also to release the ship from mapping for conducting process
556 rate experiments. Most importantly, a detailed analysis of errors from sampling methods and
557 designs must be taken prior to a cruise so that potential errors can be estimated and possibly
558 avoid.

559 **SUMMARY**

560 The high resolution observations of physical-biological fields obtained in the California
561 Current system off Oregon during June 2002 revealed the strong correlations between coastal
562 upwelling areas and zooplankton biomass maxima. Primary productivity in the coastal region
563 off Oregon is enhanced by upwelling, which supports the ecosystem in the region. However the
564 zooplankton productivity within the region not only depends on local growth and regeneration,

565 but also the convergence of zooplankton biomass gradient advection. In the coastal area
566 shallower than the 153 m isobaths between 41°44'N and 44°37'N, the mesozooplankton biomass
567 was approximately 4×10^4 ton C. There are significant differences in transport flux estimates
568 from different current fields based on Barnes and BDF interpolation methods indicating inherent
569 uncertainties from the field data and the importance to resolve these differences in field. In spite
570 of these discrepancies, the results indicate the influx of zooplankton biomass into the coastal area
571 occurred primarily at the northern boundary at Newport, Oregon by the southward California
572 Current approximately $1 - 2.5 \times 10^3$ ton C d^{-1} at a rate of 0.03–0.06 day^{-1} based on two different
573 analytical methods which are close to the mean growth rate of zooplankton (Huntley & Lopez
574 1992; Hirst & Bunker, 2003; Bi et al. 2010; Zhou et al. 2010). The flux at the southern boundary
575 is one order of magnitude less than that of the northern boundary. The offshore transport of high
576 zooplankton biomass water was found off Heceta Bank and Cape Blanco while the onshore
577 intrusions of low zooplankton biomass waters were found between Heceta Bank and Coos Bay.
578 The net offshore transport of zooplankton crossing the 153 m isobaths was approximately 0.8–
579 3.7×10^3 ton C d^{-1} at a rate of 0.02–0.09 day^{-1} significantly contributing to the loss of coastal
580 communities during June 2002. Thus in the Oregon coast, the physical advection processes are
581 on the same order of magnitude of zooplankton growth rate, and of important processes in
582 determining zooplankton retention and productivity.

583

584 **ACKNOWLEDGEMENTS**

585 We would like to thank the Oregon State University Marine tech group and crew of the R/V
586 Thomas Thompson for providing technical support in instrument integration. M. Zhou and D.
587 Wu are also grateful for the zooplankton data provided by Dr. W. Peterson and his group. This
588 research was supported by the United States National Science Foundation grant numbers
589 OCE0002257 and OCE 0435581 to M. Zhou and OCE0435619 to T. Cowles.

590

591

592
593
594
595
596
597
598
599
600
601
602
603
604
605
606
607
608
609
610
611
612

LITERATURE CITED

Barnes SL (1964) A technique for maximizing details in numerical map analysis. *J Appl Meteor* 3: 396–409.

Barth JA, Pierce SD, Smith RL (2000) A separating coastal upwelling jet at Cape Blanco, Oregon and its connection to the California Current System. *Deep-Sea Res II* 47: 783–810.

Barth JA, Cowles TJ, Korso PM, Shearman RK (2002) Injection of carbon from the shelf to offshore beneath the euphotic zone in the California Current. *J Geophys Res* 107: doi:10.1029/2001JC000956.

Barth JA, Pierce SD, Cowles TJ (2005) Mesoscale structure and its seasonal evolution in the northern California Current system. *Deep-Sea Res II* 52: 5–28.

Benfield MC, Lavery AC, Wiebe PH, Greene CH, Stanton TK, Copley NJ (2003) Distributions of physonect siphonulae in the Gulf of Maine and their potential as important sources of acoustic scattering. *Can J Fish Aquat Sci* 60: 759–772.

Benoit-Bird KJ, Aub WWL (2003) Echo strength and density structure of Hawaiian mesopelagic boundary community patches. *J Acoust Soc Am* 114: 188–1897.

Beyer WH (1987) *Handbook of Mathematical Sciences*, CRC Press.

Bi H, Feinberg L, Shaw C T, Peterson WT (2010) Estimated development times for stage-structured marine organisms are biased if based only on survivors, *J Plankton Res* 33: 751-762.

Brink KH, Cowles TJ (1991) The coastal transition zone program. *J Geophys Res* 96: 14,637–14,647.

613 Bretherton FP, Davis RE, Fandry CB (1976) A technique for objective analysis and design of
614 oceanographic experiments applied to MODE-73. *Deep-Sea Res* 23: 559–582.

615 Chereskin TK, Strub PT, Paulson C, Pillsbury D (1994) Mixed-layer observations at the offshore
616 California Current moored array. *EOS* 75: 140–141.

617 Dorland, RD, Zhou M (2008) Circulation and heat fluxes during the austral fall in George VI
618 Sound, Antarctic Peninsula. *Deep–Sea Res II* 55: 294–308.

619 Erofeeva SY (2003) Tidal currents on the central Oregon shelf: Models, data, and assimilation. *J*
620 *Geophys Res*, doi:10.1029/2002JC001615.

621 Fossheim M, Zhou M, Pedersen OP, Tande KS, Zhu Y, Edvardsen A (2005) Interactions between
622 biological and environmental structures on the coast of Northern Norway. *Mar Ecol Progr*
623 *Ser* 300: 147-158.

624 Geen AV, Takesue RK, Gooddard J, Takahashi T, Barth JA, Smith RL (2000) Carbon and nutrient
625 dynamics during coastal upwelling off Cape Blanco, Oregon. *Deep-Sea Res II* 47: 975–
626 1002.

627 Gómez–Gutiérrez J, Peterson W (1999) Egg production rates of eight calanoid copepod species
628 during summer 1997 off Newport, Oregon USA. *J Plankton Res* 21: 637–657.

629 Haidvogel DB, Beckmann A, Hedstrom KS (1991) Dynamical simulations of filament formation
630 and evolution in the Coastal Transition Zone. *J Geophys Res* 96: 15,017–15,040.

631 Hawkins HF, Rosenthal SL (1965) On the computation of stream functions from the wind field.
632 *Monthly Weather Review* 93: 245–252.

633 Herman AW (1992) Design and calibration of a new optical plankton counter capable of sizing
634 small zooplankton. *Deep-Sea Res* 39: 395–415.

635 Hirst AG, Bunker AJ (2003) Growth of marine planktonic copepods: Global rates and patterns in
636 relation to chlorophyll a, temperature, and body weight. *Limnol Oceanogr* 48: 1988–2010.

637 Hofmann EE, Hedstrom K, Moisan JR, Haidvogel DB, Mackas DL (1991) Use of simulated
638 tracks to investigate general transport patterns and residence times in the coastal transition
639 zone. *J Geophys Res* 96: 15,041–15052.

640 Huntley ME, Gorzalez A, Zhu Y, Zhou M, Irigoien X (2000) Zooplankton dynamics in a
641 mesoscale eddy-jet system off California. *Mar Ecol Prog Ser* 201: 165–178.

642 Huntley ME, Lopez MDG (1992) Temperature-dependent production of marine copepods: a
643 global synthesis. *Am Nat* 140: 201–242.

644 Huntley ME, Zhou M, Norhausen W (1995) Mesoscale distribution of zooplankton in the
645 California Current in late spring observed by an Optical Plankton Counter. *J Mar Res* 53:
646 647–674.

647 Kosro PM, Huyer A (1986) CTD and velocity surveys of seaward jets off northern California,
648 July 1981 and 1982. *J Geophys Res* 91: 7680–7690.

649 Kosro PM, Ramp SR, Smith RL, Chavez FP, Cowles TJ, Abbott MR, Strub PT, Barber RT,
650 Jessen P, Small LF (1991) The structure of Transition Zone between coastal waters and
651 open ocean off northern California winter and spring 1987. *J Geophys Res* 98: 14707–
652 14730.

653 Kundu PK, Allen JS (1976) Some three-dimensional characteristics of low-frequency current
654 fluctuation near the Oregon coast. *J Phys Oceanogr* 6: 181–199.

655 Magnell BA, Winant CD (1993) Subtidal circulation over the northern California shelf. *J*
656 *Geophys Res* 98: 18,147–18,180.

657 Mackas DL, Washburn L, Smith SL (1991) Zooplankton community pattern associated with a
658 California Current cold filament. *J Geophys Res* 96: 14,781–14,797.

659 McCreary JP, Fukamachi Y, Kundu PK (1991) A numerical investigation of jets and eddies near
660 an eastern ocean boundary. *J Geophys Res* 96: 2515–2534.

661 Peterson WT, Keister JE (2002) The effect of a large cape on distribution patterns of coastal and
662 oceanic copepods off Oregon and northern California during the 1998-1999 El Nino-La
663 Nina. *Prog Oceanogr* 53: 389–411.

664 Peterson WT, Gomez-Gutierrez J, Morgan CA (2002) Cross-shelf variation in calanoid copepod
665 production during summer 1996 off the Oregon coast, USA. *Mar Bio* 141: 353–365.

666 Pickett MH, Paduan JD (2003) Ekman transport and pumping in the California Current based on
667 U.S. Navy's high-resolution atmospheric model (COAMPS). *J Geophys Res*,
668 doi:10.1029/2003JC001902.

669 Pierce SD, Allen JS, Walstad LJ (1991) Dynamics of the Coastal Transition Zone Jet, 1. Linear
670 Stability Analysis. *J Geophys Res* 96: 14,979–14,994.

671 Pierce SD, Smith RL, Kosro PM, Barth JA, Wilson CD (2000) Continuity of the poleward
672 undercurrent along the eastern boundary of the mid-latitude north Pacific. *Deep-Sea Res II*
673 47: 811–829.

674 Platt T, Denman K (1978) The structure of pelagic marine ecosystems. *Rapp. P.-V. Re ´un. Cons.*
675 *Int. Explor Mer.* 173: 60–65.

676 Rienecker MM, Mooers CNK (1989) Mesoscale eddies, jets, and fronts off Point Arena,
677 California, July 1986. *J Geophys Res* 94: 12,555–12,569.

678 Rodriguez J, Mullin MM (1986) Relation between biomass and body weight of plankton in a

679 steady state oceanic ecosystem. *Limnol Oceanogr* 31: 361–370.

680 Rudnick DL (1996) Intensive surveys of the Azores front. 2: Inferring the geostrophic and
681 vertical velocity fields. *J Geophys Res* 101: 16291–16303.

682 Shearman RK, Barth JA, Allen JS, Haney RL (2000) Diagnosis of the three-dimensional
683 circulation in mesoscale features with large Rossby number. *J Phys Oceanogr* 30: 2687–
684 2709.

685 Sheldon RW, Parsons TR (1967) A Continuous size spectrum for particulate matter in the sea. *J*
686 *Fish Res Board Can* 24: 909–915.

687 Sheldon RW, Prakash A, Sutcliffe WHJ (1972) The size distribution of particles in the ocean.
688 *Limnol Oceanogr* 17: 327–340.

689 Small LF, Menzies DW (1981) Patterns of primary productivity and biomass in a coastal
690 upwelling region. *Deep Sea Res I* 28:123–149.

691 Sprules WG, Munawar M (1986) Plankton size spectra in relation to ecosystem productivity, size
692 and perturbation. *Can J Fish Aquat Sci* 43: 1789–1794.

693 Silvert W, Platt T (1977) Energy flux in the pelagic ecosystem. *Limnol Oceanogr* 23: 813–816.

694 Strub PT, Kosro PM, Huyer A (1978) The nature of the cold filaments in the California Current
695 System. *J Geophys Res* 96: 14,743–14,768.

696 Ullman DS, Dale AC, Hebert D, Barth JA (2003) The front on the northern flank of Georges
697 Bank in spring: 2. Cross-frontal fluxes and mixing. *J Geophys Res* doi:10.1029
698 /2002JC1328.

699 Washburn L, Kadko DC, Jones BH, Hayward T, Kosro PM, Stanton TP, Ramp S, Cowles TJ

700 (1991) Water mass subduction and the transport of phytoplankton in a coastal upwelling
701 region. *J Geophys Res* 96: 14,927-14,946.

702 Wiebe PH, Beardsley RC,, Bucklin A, Mountain DG (2001) Coupled biological and physical
703 studies of plankton populations in the Georges Bank region and related North Atlantic
704 GLOBEC study sites. *Deep-Sea Res II*, 1–2.

705 Zhou, M, Carlotti F, Zhu Y (2010) A size-spectrum zooplankton closure for ecosystem models. *J*
706 *Plankton Res* 32: 1147–1165.

707 Zhou M, Huntley ME (1997) Population dynamics theory of plankton based on biomass spectra.
708 *Mar Ecol Prog Ser* 159: 61–73.

709 Zhou M (1998) An objective interpolation method for spatiotemporal distribution of marine
710 plankton. *Mar Ecol Prog Ser* 174: 197–206.

711 Zhou M, Tande KS, Zhu Y, Basedow S (2009) Productivity, trophic levels and size spectra of
712 zooplankton in northern Norwegian shelf regions. *Deep–Sea Res II* 56: 1934–1944.

713 Zhou M, Zhu Y, Putnam S, Peterson J (2001) Mesoscale variability of physical and biological
714 fields in southeastern Lake Superior. *Limnol Oceanogr* 46: 679–688.

715 Zhou M, Zhu Y, Tande KS (2005) Circulation and behavior of euphausiids in Norwegian sub-
716 Arctic fjords. *Mar Ecol Prog Ser* 300: 159-178.

717 Zhu Y, Tande KS, Zhou M (2009) Mesoscale physical processes and zooplankton productivity in
718 the northern Norwegian shelf region. *Deep–Sea Res II* 56: 1922-1933.

719

720

721 Table 1. Zooplankton biomass transport fluxes ($\times 10^3$ ton C d^{-1}) into the coastal area shallower
722 than 153 m isobaths between 41°44'N (Transect 12) and 44°37'N (Transect 1) (Fig. 1) and
723 corresponding rates (d^{-1}). A positive or negative value represents a net flux of biomass into or
724 out of the coastal area. The rate estimate is based on the estimated total standing biomass of
725 4×10^4 ton C within the control area.

726

727 **Table 1.**

Current field	Transect 1		Transect 12		153 m		Net	
	Flux	Rate	Flux	Rate	Flux	Rate	Flux	Rate
Detided ADCP currents	2.1	0.05	0.1	0.003	1.4	0.04	3.6	0.09
Streamfunction ¹	2.5	0.06	-0.2	-0.005	-3.7	-0.09	-1.4	-0.04
Streamfunction ²	1.0	0.03	0.1	0.003	-0.8	-0.02	0.3	0.01

728 ¹ The streamfunction is derived from an isotropic covariance function with a scale of 50 km.

729 ² The streamfunction is derived from an anisotropic covariance function with a zonal scale of 33
730 km and a meridional scale of 88 km.

731

732

733 **Figure Captions**

734 Fig. 1. Bathymetry of the study area off Oregon. The thin black lines are isobaths of 50, 100,
735 153 and 2000 m, the thick black lines are mesoscale survey transects from 1 to 7 and
736 southern fine-scale survey transects from 8 to 12 indicated by the labels next to these lines,
737 and the black cross at Transect 1 indicates the location of NDBC buoy 46050.

738 Fig. 2. Autocorrelations calculated from temperature data: (a) zonal and (b) meridional
739 components. The black dots are calculated data, the dash lines are the best-fit covariance
740 function $(1-r)e^{-r}$, and the solid lines are the best-fit covariance function $(1-r^2)e^{-r^2}$. The
741 zero crossings are 33 km and 88 km in the zonal and meridional directions, respectively.

742 Fig. 3. The time series of wind measurements at NOAA NDBC buoy 46050 during the survey
743 period: (a) wind speed, (b) zonal component and (c) meridional component. The shaded
744 areas indicate the periods of the mesoscale, northern and southern fine-scale surveys.

745 Fig. 4. Horizontal distributions at 5 m: (a) temperature in °C represented by false colors with
746 black dash contours at 1°C intervals, (b) chlorophyll in mg m^{-3} represented by false colors
747 with black dash contours at 1 mg m^{-3} intervals, and (c) zooplankton biomass in mg C m^{-3}
748 represented by false colors and zooplankton abundance in individuals m^{-3} represented by
749 solid black contours. The solid white contour lines indicate the 153 m isobath.

750 Fig. 5. Horizontal current distributions at 25 m in m s^{-1} represented by vectors: (a) 30 minute
751 averaged detided ADCP currents, (b) currents derived from Barnes interpolation, (c)
752 currents derived from the BDF interpolation. The solid contour lines indicate the 153 m
753 isobath.

754 Fig. 6. Depth averaged distributions between 0 and 153 m: (a) zooplankton abundance in
755 individual m^{-3} and (b) zooplankton biomass in mg C m^{-3} represented by false colors. The

756 numbers 1–6 in (a) are used to mark the six $20 \times 20 \text{ km}^2$ areas representing: 1) the
757 southward jet area in the northern boundary, 2) the high biomass area on Heceta Bank, 3)
758 the high biomass area within the southwestward jet off Heceta Bank, 4) the low biomass
759 area within the onshore return flow, 5) the high biomass area in the coastal region north of
760 Cape Blanco, and 6) the high biomass area within the offshore jet south of Cape Blanco.

761 Fig. 7. Cross-shelf vertical transects along mesoscale Transect 5: (a) temperature in $^{\circ}\text{C}$
762 represented in false colors with ADCP currents represented by the horizontal vectors for
763 the zonal components and the 45° vectors for the meridional components, (b) chlorophyll
764 in mg m^{-3} represented in false colors, and (c) zooplankton biomass in mg C m^{-3}
765 represented in false colors and zooplankton abundance in individuals m^{-3} represented by
766 solid black contours.

767 Fig. 8. Depth (0–153 m) integrated zooplankton biomass horizontal transport in $\text{mg C m}^{-1} \text{ s}^{-1}$:
768 (a) the transport derived from 30 minute averaged detided ADCP currents, (b) the transport
769 derived from the Barnes interpolation, and (c) the transport derived from the BDF
770 interpolation. The solid contour lines indicate the 153 m isobath.

771 Fig. 9. Depth (0–153 m) integrated biomass gradient advection: (a) the biomass gradient
772 advection in $\text{mg C m}^{-2} \text{ s}^{-1}$ derived from the BDF interpolation, and (b) the specific rate of
773 biomass gradient advection in day^{-1} based on the ratio of the depth integrated biomass
774 gradient advection to the depth integrated biomass. The dash lines indicate the zero
775 contours.

776 Fig. 10. Biomass spectra from OPC measurements: (a) Areas 1 and 4, (b) Areas 2 and 5, (c)
777 Areas 3 and 6, and (d) daytime (05:00–19:00 h) and nighttime (19:00–05:00 h) in the
778 survey area deeper than 153 m. The areas are indicated in Fig. 6a. The dots represent the

779 means and solid vertical lines indicate 95% confidence intervals.

780 Fig. 11. Percentage composition of dominant zooplankton species from zooplankton samples
781 collected in Area 2 indicated in Fig. 6a.

782 Fig. 12. Depth centers of zooplankton biomass derived from individual vertical profiles in the
783 survey area deeper than 153 m as a function of nighttime (19:00–05:00) represented by
784 open circles and daytime (05:00–19:00) represented by solid gray dots. The solid black
785 dots represent the hourly means and the vertical black lines are their standard deviations.

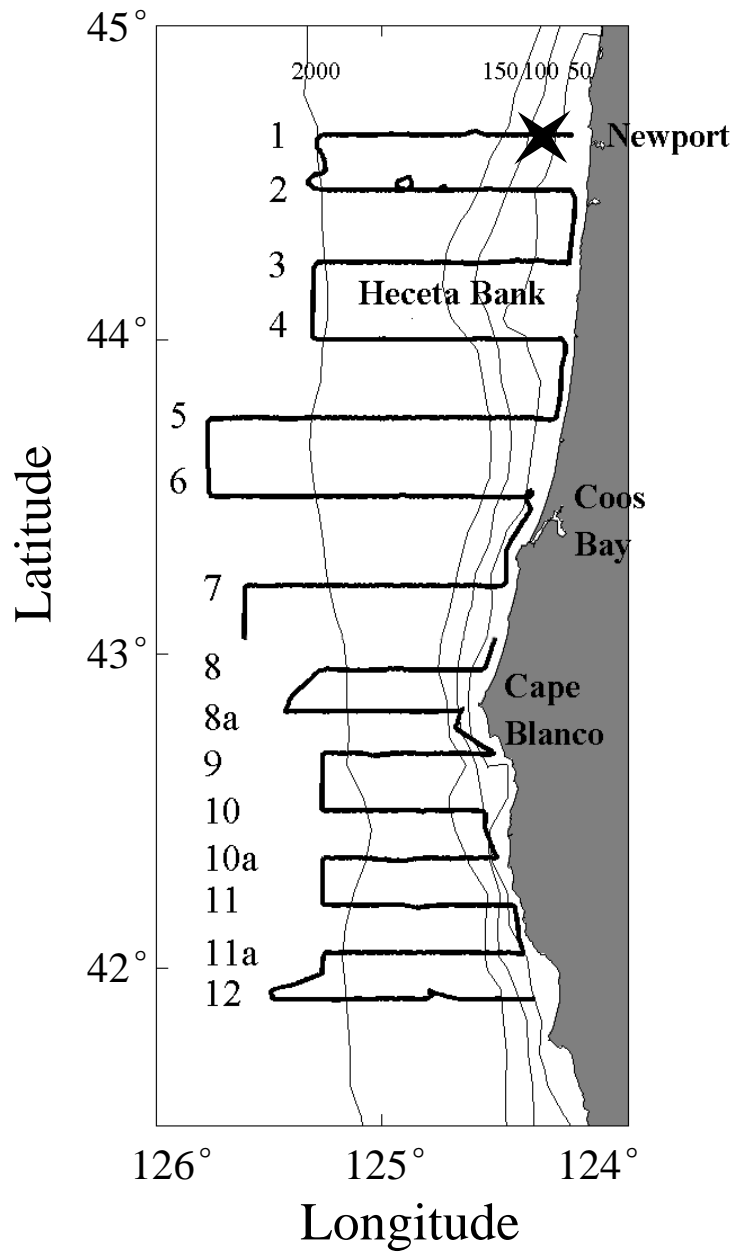


Fig. 1

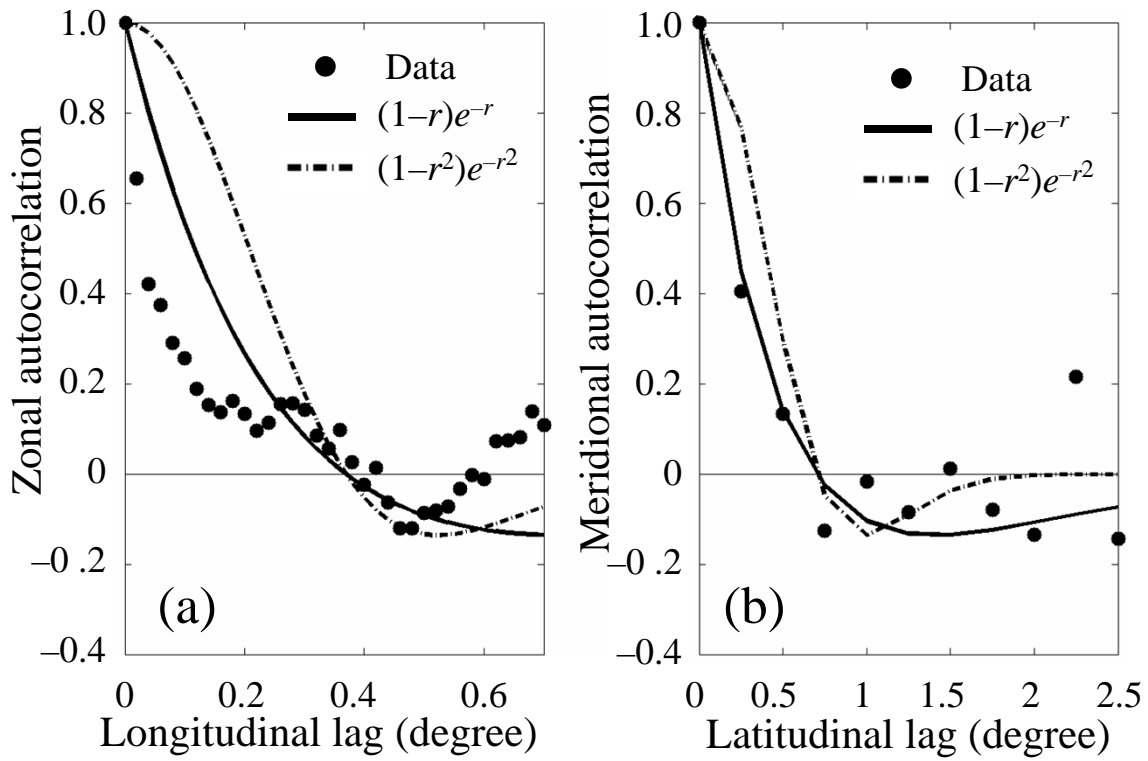


Fig. 2

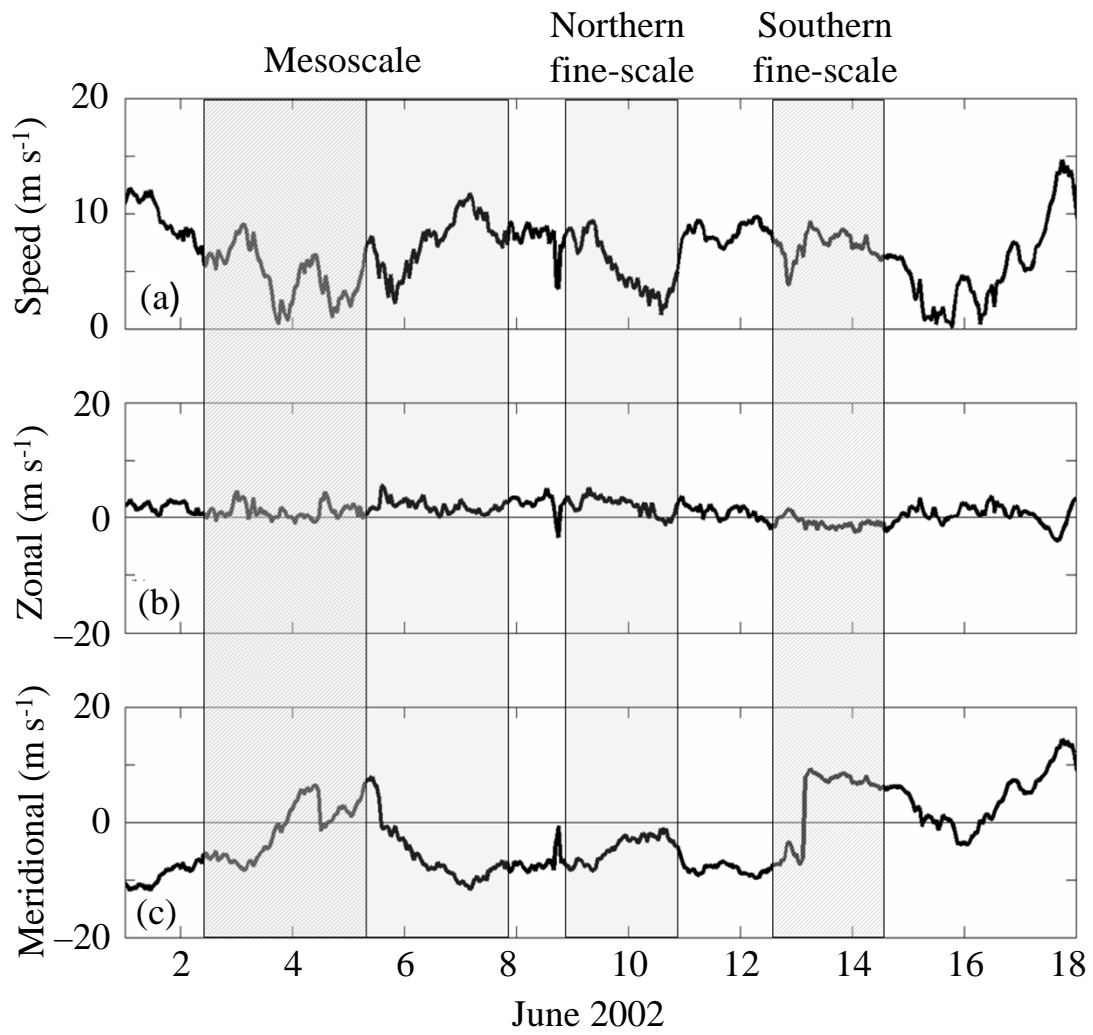


Fig. 3

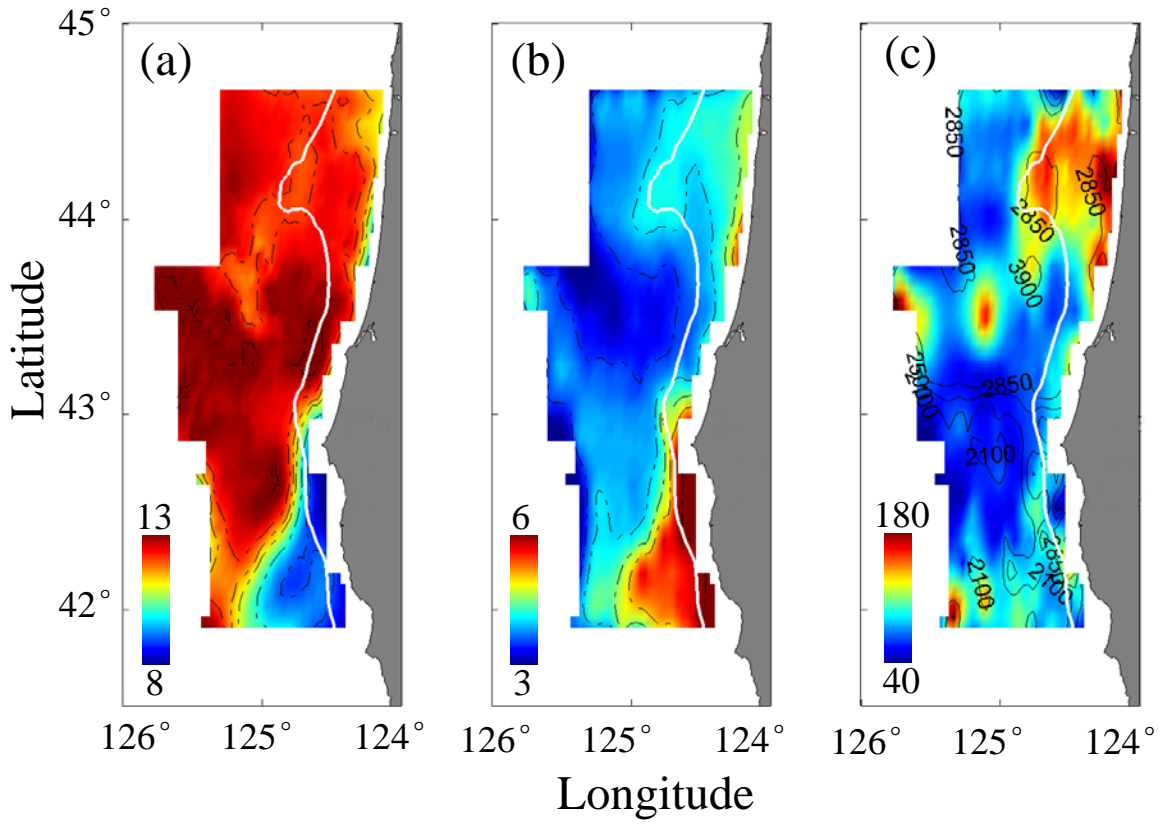


Fig. 4

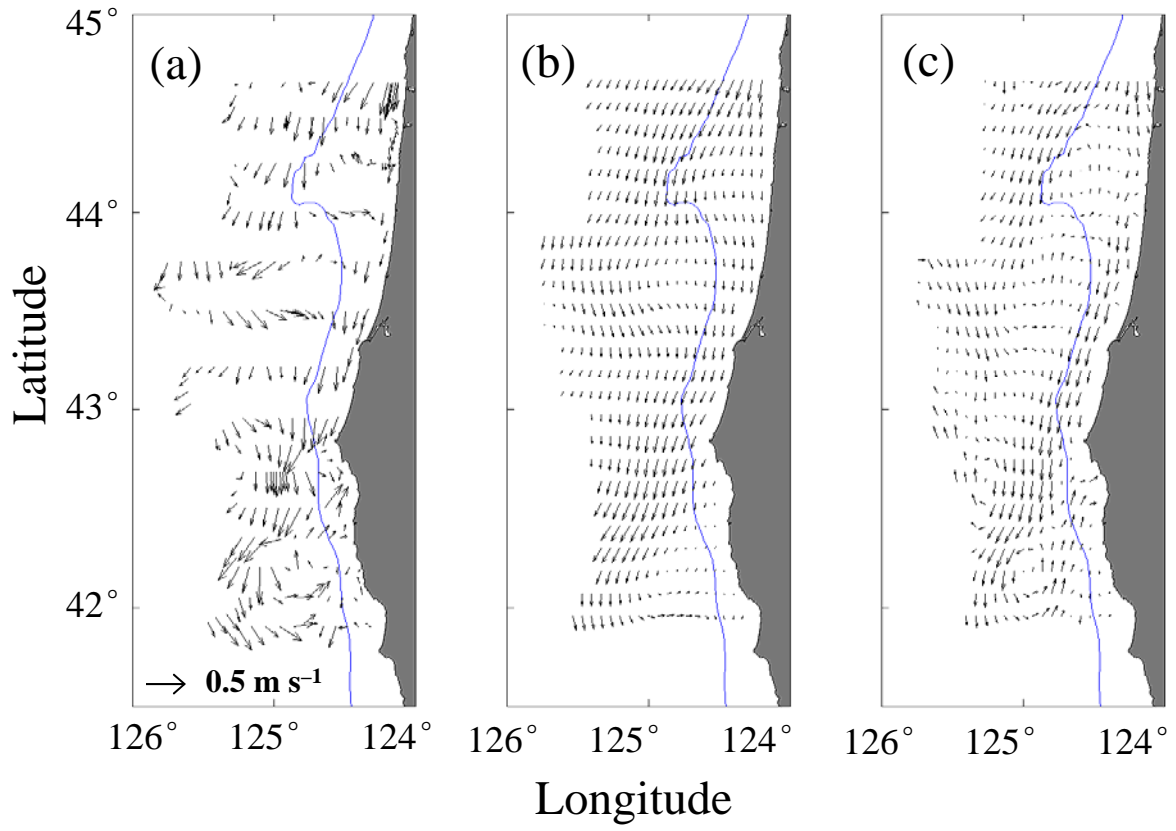


Fig. 5

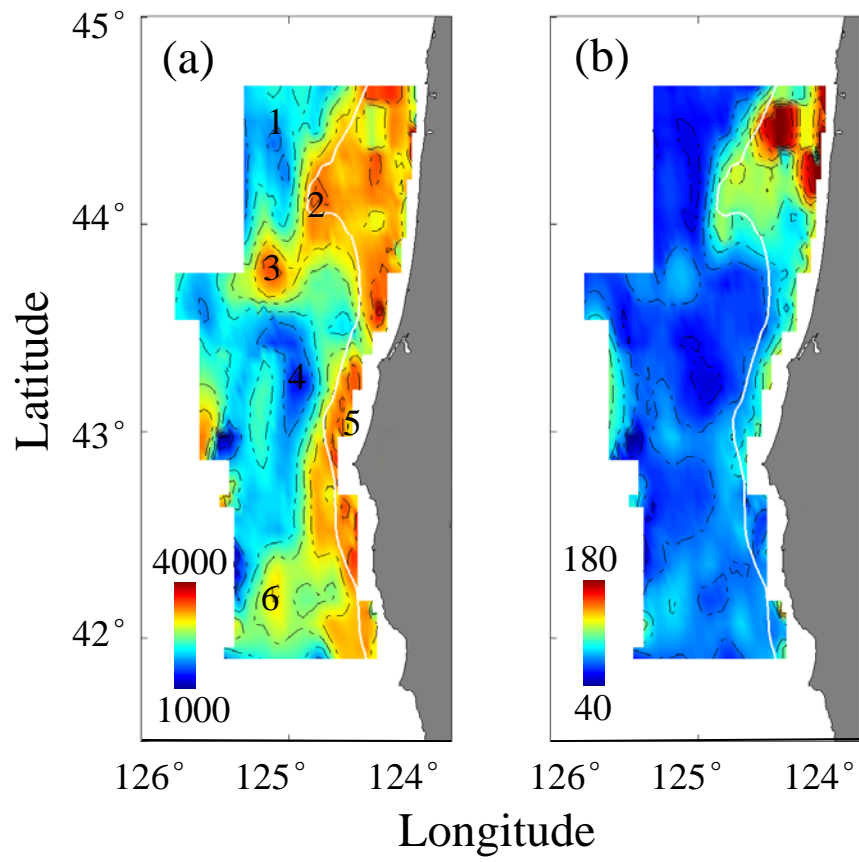


Fig. 6

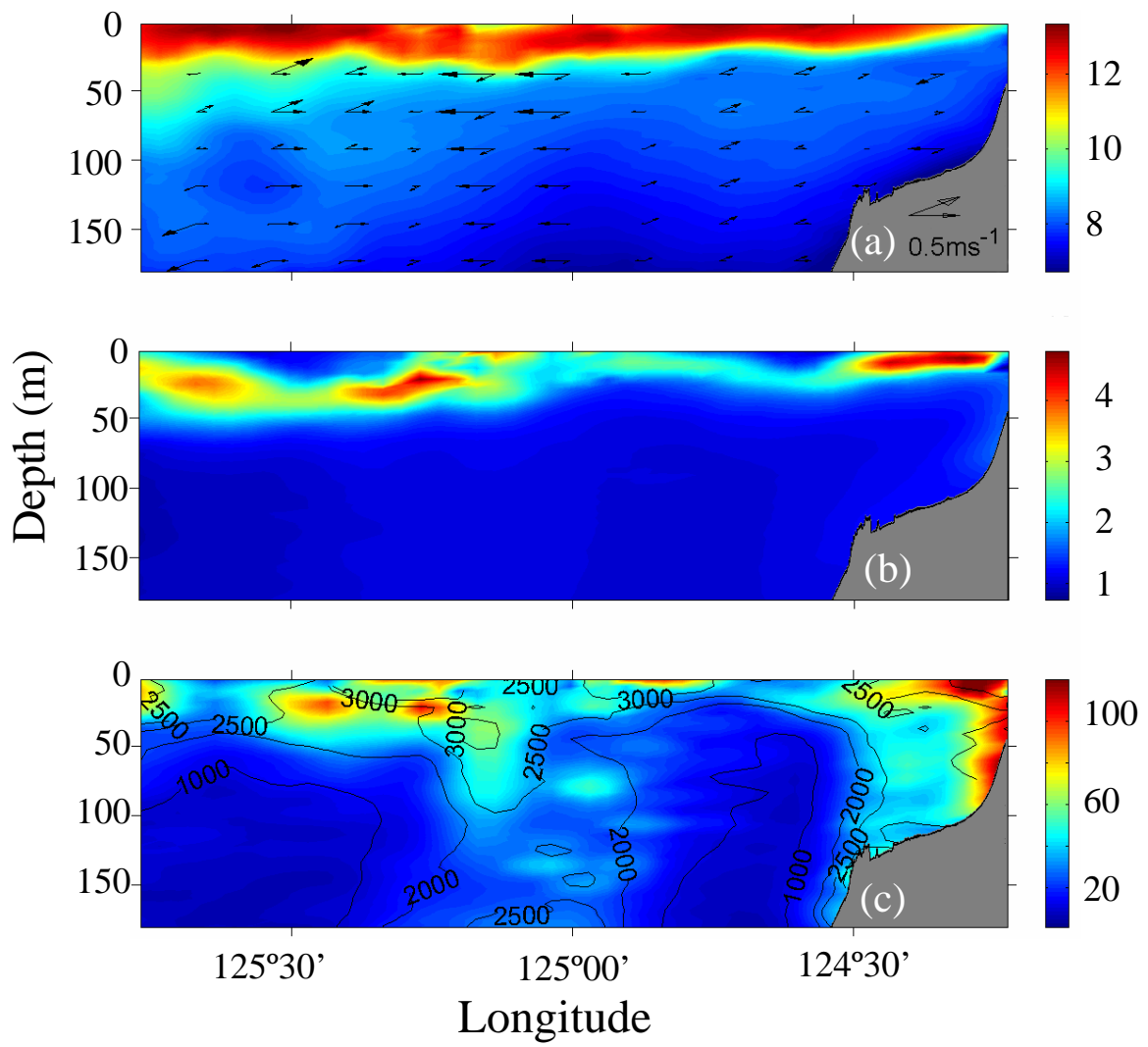


Fig. 7

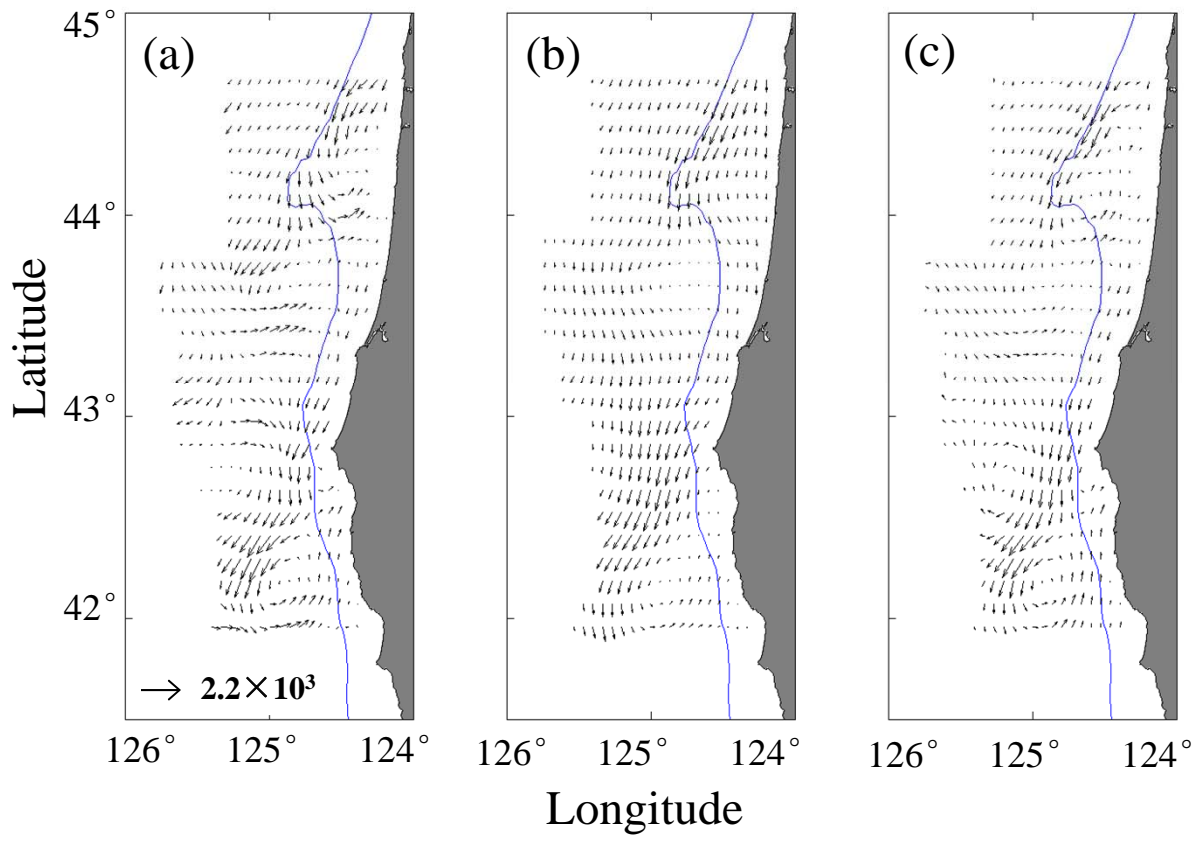


Fig. 8

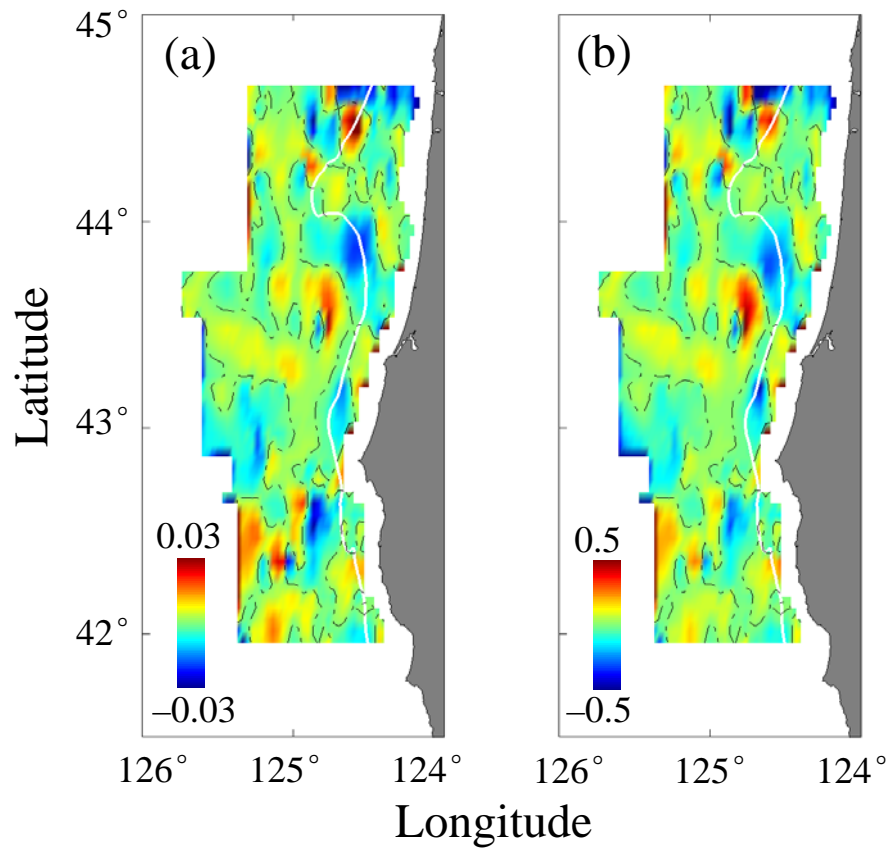


Fig. 9

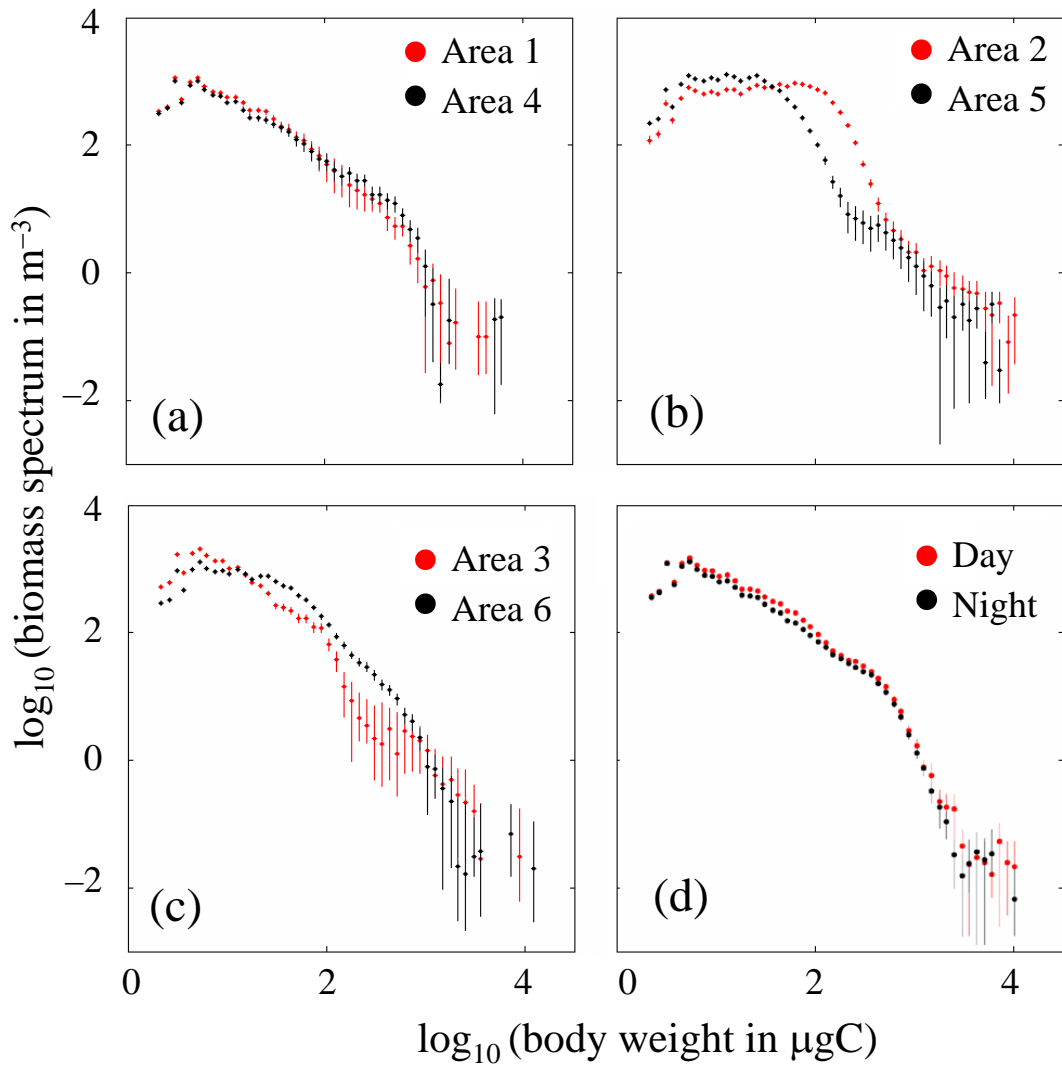


Fig. 10

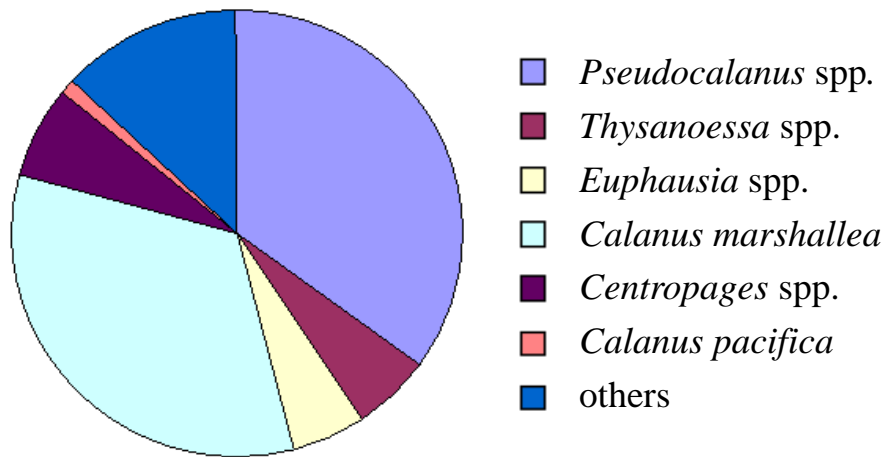


Fig. 11

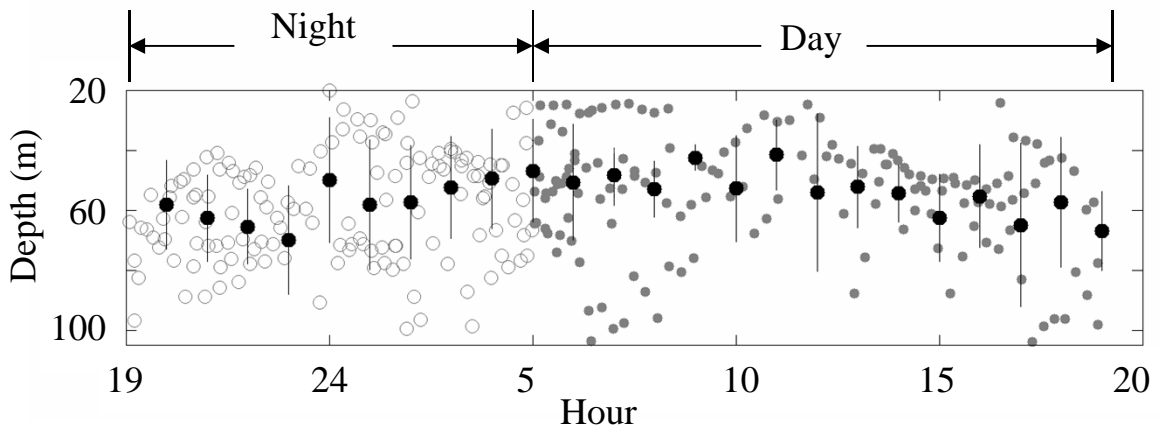


Fig. 12